Remote Sensing of Environment 159 (2015) 14–27

Contents lists available at ScienceDirect

Remote Sensing of Environment

journal homepage: www.elsevier.com/locate/rse

Characterizing the uncertainties in spectral remote sensing reflectance for SeaWiFS and MODIS-Aqua based on global in situ matchup data sets

Timothy S. Moore *, Janet W. Campbell, Hui Feng

Ocean Process Analysis Laboratory, University of New Hampshire, Durham, NH 03824, USA

ARTICLE INFO

Article history:
Received 22 April 2014
Received in revised form 13 November 2014
Accepted 28 November 2014
Available online 29 December 2014

Keywords:
Ocean color
Remote sensing
Validation
Bio-optics
Uncertainties

ABSTRACT

Uncertainties in the spectral remote-sensing reflectance for SeaWiFS and MODIS-Aqua are characterized based on globally distributed data sets of in situ/satellite matchups. The in situ data sets were derived from fixed mooring sites and ship data using a variety of field radiometers. An optical classification procedure was applied to the satellite reflectance from each matchup pair to derive its fuzzy membership to eight previously characterized, optical water types. The memberships were then used as weights to derive uncertainty measures for the optical water types. The resulting uncertainty measures are shown to vary by optical water type for both sensors. Overall, the root-mean-square difference (RMSD) for open ocean waters is low and diminishes with increasing wavelength. The RMSD increases with optical complexity and is the highest in coastal waters associated with highly absorbing or highly scattering conditions. Although it plays a small role in RMSD, a spectral bias with a distinct zigzag pattern was detected across all water types. The most sensitive measure associated with optical water types is the relative uncertainty, which is shown to be near the desired 5% threshold for much of the open ocean for both SeaWiFS and MODIS-Aqua, but exceeds 50% in waters where the reflectance signal is low. This approach provides an objective method for characterizing uncertainty in water environments with distinct optical properties, and the results can be used in the processing of future satellite data to derive their associated uncertainty fields.

1. Introduction

Ocean color satellites provide records of various optical and biogeochemical properties of the upper layer of the global oceans. Historically, beginning in 1978 with the Coastal Zone Color Scanner, the main ocean color data product has been the chlorophyll-*a* concentration (Hu & Campbell, 2014, Chap. 7). Today, there are many more ocean color products available and include information on inherent optical properties (e.g., absorption and scattering), phytoplankton physiology (e.g., fluorescence), and carbon-related properties such as particulate organic carbon and colored dissolved organic matter. All of these products are derived from the spectral water-leaving radiance or its transformed counterpart — the remote-sensing reflectance (R_{rs}). Therefore, the precision of water-leaving radiance is of critical importance to the accuracy of all ocean color products.

Long-term records of climate variables derived from ocean color will require multi-platform measurements that are unified into a single data set (Barnes et al., 2003; National Research Council, 2011). In order to produce and interpret the records of *merged* ocean color products from multiple sensors (Maritorena & Siegel, 2005; Melin, Zibordi, & Djavidnia, 2009), the uncertainties in the water-leaving radiances need to be characterized for all sensors (Barnes et al., 2003). Furthermore, since the uncertainties have been shown to vary between open-ocean and coastal waters (Bailey & Werdell, 2006), it is important to characterize their spatial distribution.

The use of in situ data is critical for sustaining and assuring the quality of ocean color products. Measurements of water-leaving radiance at the Marine Optical Buoy (MOBY) site near Hawaii have been used in the vicarious calibration of both SeaWiFS and MODIS-Aqua (Bailey, Hooker, Antoine, Franz, & Werdell, 2008; Clark et al., 2002). In this procedure, in situ water-leaving radiances are 'backed out' of the atmosphere using atmospheric correction codes in reverse, and compared to the satellite top-of-atmosphere (TOA) radiances. A correction factor is then applied to force the TOA radiances to agree with the MOBY-derived TOA radiances. This procedure corrects for (or minimizes) systematic biases inherent in the sensor and in the atmospheric correction algorithm (Franz, Bailey, Werdell, & McClain, 2007).

In situ data are also used to evaluate the accuracy of derived products, including water-leaving radiance. This is achieved through matchup analyses involving in situ data matched closely in time and space to the satellite measurement. For satellite radiances, a wide variety of moored radiometers are now operating with the advantage of providing continuous measurements that increase the temporal aspect of matchups.

* Corresponding author at: Ocean Process Analysis Laboratory, University of New Hampshire, USA. Tel.: +1 603 862 0690.
E-mail address: timothy.moore@unh.edu (T.S. Moore).

http://dx.doi.org/10.1016/j.rse.2014.11.025
0034-4257/

An issue with the matchup approach has always been the limitations in data coverage over time and space. Though less stringent than the criteria used for vicarious calibration matchups, the criteria used for validation purposes result in only about 15% of potential matchup points being suitable for this type of assessment (Bailey & Werdell, 2006). Thus, large collections of data are needed. In addition, diversity in the range of environmental conditions is desired to assess the full dynamic range of the satellite product for complete uncertainty characterization.

Lack of sufficient matchup data has led to other approaches, such as those based on satellite-to-satellite comparisons (Hu, Feng, & Lee, 2013; Melin, 2010) or the propagation of errors through models (e.g., Aurin, Mannino, & Franz, 2013; Maritorena & Siegel, 2005). While a satellite-only based analysis overcomes the sampling issue, an inherent limitation is that it does not capture any bias or systematic errors that might exist in both satellite records. An error in the atmospheric correction algorithm applied to two sensors, for example, would not be detected by comparing their satellite records.

It has been the goal of NASA to achieve 5% accuracy for water-leaving radiance in blue bands (e.g., 443 nm) for its sensors, including SeaWiFS and MODIS-Aqua (Bailey & Werdell, 2006; Hooker, Esaias, Feldman, Gregg, & McClain, 1992). Hu et al. (2013) reported that open-ocean radiance uncertainties are at or near the 5% goal, based on a satellite-only analysis of SeaWiFS and MODIS-Aqua data, but they conclude that their estimates are lower bounds. Reported values for relative uncertainty based on matchup analyses range from 10 to 21% (Antoine et al., 2008; Bailey & Werdell, 2006; Melin et al., 2009; Zibordi, Melin, & Berthon, 2006). Bailey and Werdell (2006) showed that uncertainties varied between deep-ocean and coastal areas based on a distributed global data set, thus demonstrating that the range in accuracy varies in relation to water environment and geographic region. Overall, these collective results indicate a variation in uncertainties between open-ocean and coastal regions. Furthermore, any global assessment of uncertainty based on in situ data must correct for the disproportionately large amount of data in coastal regions as compared to the global ocean area (Moore, Campbell, & Dowell, 2009).

In this study, we employ comprehensive, globally distributed validation data sets for satellite-derived remote sensing reflectance from the NASA SeaWiFS Bio-optical Archive and Storage System (SeaBASS) for SeaWiFS and MODIS-Aqua. The in situ data sets are assemblages of buoy, tower, and ship data and cover a large range of optical environments. We explore the distribution of uncertainties by *optical water type* (OWT). We have previously characterized the empirical chlorophyll product with this approach (Moore et al., 2009), and here we apply the method to reflectance matchup data sets for SeaWiFS and MODIS-Aqua to quantify uncertainties in the satellite remote-sensing reflectance. This approach provides an objective method for characterizing uncertainty in water environments with distinct optical properties, and the results can be used in the processing of future satellite data to derive their associated uncertainty fields. In addition, the method also provides a common reference point for comparison between sensors, which can be useful for merging satellite data into climatological records.

2. Methods

2.1. Data sets

The in situ data used in this analysis were obtained from NASA's SeaBASS optical database (Werdell et al., 2003). They were derived from the following sources (Table 1): the fixed Marine Optical Buoy (MOBY) off the Hawaiian island of Lanai, the fixed BOUSSOLE mooring site in the Mediterranean Sea (Antoine et al., 2008), fixed stations from the AERONET-OC network (Holben et al., 1998; Zibordi et al., 2009) at various coastal sites and one freshwater site (Palgrunden), and from ships contributed by various investigators.

SeaWiFS and MODIS-Aqua R_{rs} data were matched with the in situ data using the SeaBASS web interface at http://seabass.gsfc.nasa.gov/seabasscgi/search.cgi to create validation data sets. The returned validation data sets cover a period from 1997 through 2010 for SeaWiFS, and 2002 through 2012 for MODIS-Aqua. Matchup points from MOBY that were used in the vicarious calibration were removed from the validation data pool and analyzed separately. The processing versions of the satellite data were R2010.0 for SeaWiFS and R2013.1 for MODIS-Aqua. Dedicated web pages containing the specific details and further information on all reprocessings by mission, including the R2010.0 processing for SeaWiFS and R2013.1 for MODIS-Aqua, can be found through the NASA ocean color website http://oceancolor.gsfc.nasa.gov/.

Table 1
The number of stations in the SeaWiFS and MODIS-Aqua reflectance validation data sets from SeaBASS by data source.

In situ data source	SeaWiFS		MODIS-Aqua		Reference[a]
	N	Dates	N	Dates	
Ship	768	1997–2007	249	2002–2012	Werdell and Bailey (2005) and Werdell et al. (2003)
BOUSSOLE	168	2002–2007	283	2003–2007	Antoine et al. (2008)
Aeronet-OC	712	2004–2010	1050	2002–2011	Zibordi et al. (2009) and Holben et al. (1998)
MOBY	509	1997–2010	321	2002–2012	Clark et al. (2003) and Franz et al. (2007)
Total	2159		1903		

[a] Investigators responsible for providing the in situ data are listed in the Acknowledgments.

The atmospheric correction algorithm used for the satellite data sets followed that of Franz et al. (2007) as modified by Bailey, Franz, and Werdell (2010). It applies a revised version of the NIR-iterative scheme to account for particle backscattering (Siegel, Wang, Maritorena, & Robinson, 2000) using a backscattering term that contains a variable slope, as well as a simplified estimate for absorption in the red/NIR region.

A bi-directional correction based on viewing geometry and the particle phase-function (Morel, Antoine, & Gentili, 2002) was applied to both in situ and satellite reflectance data. These corrections were applied to the satellite data during the image-level processing and to the in situ data by the Ocean Biology Processing Group (OBPG) at NASA Goddard.

These comprehensive data sets represent geographically diverse environments from open-ocean to coastal regions from all major oceans, and from a diverse set of instruments with different sensor bands. Satellite-in situ spectral band matchups were qualified if within a 3-nm window between center channels (pers. comm., Chris Procter). Satellite matchup data points were generated by averaging valid reflectance values within a 5×5 pixel box centered on the in situ data point. The criteria for point/pixel selection followed that of Bailey and Werdell (2006). These criteria include the following: plus/minus 3-hour maximum time difference between measurement and satellite overpass; a maximum satellite viewing angle of 70°; maximum solar zenith angle of 56°; a maximum wind speed of 35 m/s; a minimum of 50% valid satellite pixels in the box; and a maximum coefficient of variation (CV) of 0.15 for R_{rs} and the aerosol optical thickness (*Tau*). In practice, CVs are calculated for specific wavelengths of R_{rs} (400–570 nm) and *Tau* (860–900 nm). The median of those specific CVs was the value compared to the exclusion threshold. As such, since CV is a median, the CV for some individual wavelengths might have exceeded the exclusion threshold (0.15). When the 5×5 pixel box overlapped land, 50% of non-land pixels had to have valid data and meet the other criteria. The setting of any of the L2 flags (cloud or ice, stray light, sun glint, high TOA radiance, low radiance at 547/555 nm, and atmospheric correction failure) also led to exclusion.

2.2. Light field definitions

In this study, we are primarily dealing with the spectral remote-sensing reflectance denoted by the vector R_{rs}. The remote-sensing

reflectance in the SeaWiFS and MODIS validation data sets – both in situ and satellite – are $R_{rs}(0+)$, the remote-sensing reflectance just above the water surface, which is the standard form for NASA satellite radiance products. All statistical calculations of uncertainty are based on this form. To determine the membership of each matchup data pair to an optical water type (OWT), we transformed $R_{rs}(0+)$ to $R_{rs}(0-)$, the remote-sensing reflectance just below the water surface, using the relationship:

$$R_{rs}(0-) = \frac{R_{rs}(0+)}{0.52 + 1.7R_{rs}(0+)}. \quad (1)$$

The satellite $R_{rs}(0-)$ was used in the OWT classification. When we refer to R_{rs}, it will be in reference to the above-water form unless specifically noted.

2.3. Classification and partitioning of data

In previous work (Moore et al., 2009), eight OWTs were defined from the NASA bio-Optical Marine Algorithm Dataset (NOMAD) (Werdell & Bailey, 2005), and represent the distribution and variation of remote-sensing reflectance found across the globe. The OWTs are numbered in increasing optical complexity such that OWTs 1 through 4 correspond with case 1 waters, while OWTs 5 through 8 are consistent with case 2 waters. This sequencing is supported by the associated median diffuse attenuation coefficients at 490 nm (Kd490) derived from the original NOMAD data set partitioning, which are 0.026, 0.031, 0.045 and 0.083 m^{-1} for OWTs 1 through 4 respectively, and 0.171, 0.471 and 0.477 m^{-1} for OWTs 5 through 7 respectively (not enough data for OWT 8).

For reference and context, the global distribution of the water types is shown in Fig. 1. For this figure, daily SeaWiFS global images were classified into OWTs based on the OWT with the highest membership. The frequency of occurrence of each OWT over the entire mission lifetime (1997 to 2010) was then calculated from the number of occurrences normalized by the total number of valid points. OWTs 1 through 4 occupy the largest surface area and dominate the open oceans, while OWTs 5 through 8 occupy the smallest area and are frequently found in coastal areas. Although this was based on SeaWiFS data, a similar OWT distribution is found in MODIS-Aqua data.

The matchup data were classified into the OWTs using the procedure detailed in Moore et al. (2009). In essence, the satellite $R_{rs}(0-)$ from each data pair was used to compute a fuzzy membership to each of the eight OWTs. As the in situ measurements often contained incomplete spectral measurements (i.e., missing bands), the satellite R_{rs} data were used as input into the membership function. Matchup points with a low membership sum (<0.1), indicating a poor match to the set of optical water types defined from the NOMAD data, were excluded from the analysis. This resulted in the rejection of 10% and 11% of the initial data sets for SeaWiFS and MODIS-Aqua, respectively. The memberships were then normalized by their sum and used as weights to calculate uncertainty measures for each of the OWTs. In addition, the matchup data were sorted into OWT subsets based on the maximum membership, and color-coded scatter plots of satellite vs. in situ R_{rs} for the different OWTs were created.

2.4. Uncertainty definitions

For each matchup pair, uncertainty was defined as the difference between the satellite reflectance and the reflectance measured in situ. The root mean square difference (RMSD), bias, standard deviation, median absolute percent difference (MPD) and mean absolute percent difference (RPD) were calculated for the whole data set using the normalized fuzzy memberships as weights.

The RMSD for OWT j was calculated as:

$$RMSD_j = \sqrt{\frac{\sum_{i=1}^{N} f_{ij}\left(Rrs_{sat}^{i} - Rrs_{meas}^{i}\right)^2}{\sum_{i=1}^{N} f_{ij}}} \quad (2)$$

and the bias as:

$$bias_j = \frac{\sum_{i=1}^{N} f_{ij}\left(Rrs_{sat}^{i} - Rrs_{meas}^{i}\right)}{\sum_{i=1}^{N} f_{ij}} \quad (3)$$

where Rrs_{sat}^{i} is the satellite-derived reflectance; Rrs_{meas}^{i} is the in situ measurement (wavelength suppressed), and f_{ij} is the *normalized* membership of matchup i to OWT j ($\sum_j f_{ij} = 1$). RMSD is the preferred metric (Antoine et al., 2008) since it incorporates both the variance and the bias (Szeto, Campbell, Moore, & Werdell, 2011). Bias reveals any systematic offsets that might exist, and represents an uncertainty that cannot be removed by averaging.

The RPD and MPD are useful for assessing performance metrics set by agencies in terms of relative uncertainty. Both have been used in previous validation studies (Bailey & Werdell, 2006), and we include these for comparison with the previous estimates. We defined the RPD for OWT j as:

$$RPD_j = 100 * \frac{\sum_{i=1}^{N} f_{ij}\left|Rrs_{sat}^{i} - Rrs_{meas}^{i}\right| / Rrs_{meas}^{i}}{\sum_{i=1}^{N} f_{ij}} \quad (4)$$

and MPD as:

$$MPD_j = 100 * median\ \frac{\left|Rrs_{sat}^{i} - Rrs_{meas}^{i}\right|}{Rrs_{meas}^{i}} \quad (5)$$

where median was determined from the weighted distribution.

3. Results

3.1. Distribution of source data into OWTs based on maximum membership

To understand how source data were distributed generally, the matchup data pairs were sorted into OWTs based on the maximum membership. The OWTs were unevenly distributed among the various data sources (Table 2). Open-ocean, blue waters (OWTs 1 and 2) are predominantly MOBY data, while Aeronet-OC data are the primary source for OWTs 5 through 7. The BOUSSOLE data are largely confined to OWTs 3 and 4, while the SeaBASS ship data are distributed across all OWTs. Very few matchups were classified into OWT 8 which has the highest scattering properties. Consequently, we did not include this OWT for uncertainty calculations.

With the exception of the ship data, the other data sources represent restricted optical ranges compared to the global NOMAD-based OWTs. This highlights the difficulty in representing the full range of optical conditions from any single data source or location. Percentages of the global ocean area occupied by the OWTs based on the SeaWiFS and MODIS-Aqua climatologies are also listed in Table 2. These values were subsequently used as weights to derive global uncertainty measures.

The numbers of matchup points were also unevenly distributed across wavelengths within each optical water type (Table 3). In some cases, the number of points available for a given wavelength was low (e.g., the 547 nm band of MODIS-Aqua has fewer than 20 matchup points in OWTs 3, 4 or 5). As will be shown, metrics for these bands exhibit much higher uncertainties relative to other bands.

The sorted matchup data, color-coded according to the OWT with the highest membership, are shown in Figs. 2 and 3 for SeaWiFS and

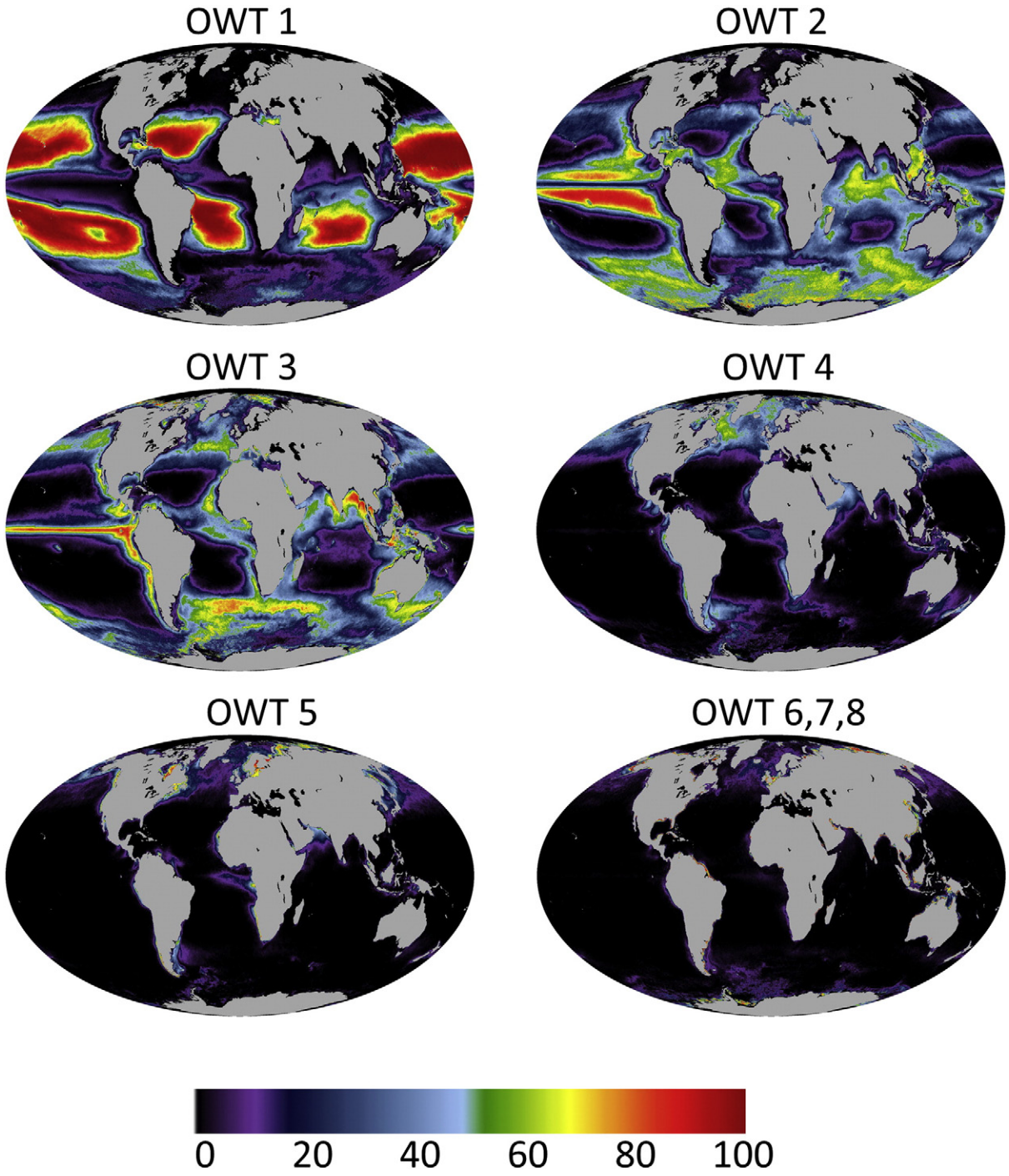

Fig. 1. Frequency of the OWTs having the highest membership derived from SeaWiFS global daily imagery from 1997 to 2010.

MODIS-Aqua, respectively. It is apparent that SeaWiFS data exhibit more scatter about the one-to-one line compared to MODIS-Aqua. They also show how the OWTs differ with respect to their spectral properties.

3.2. Distribution of uncertainty across the optical water types

All uncertainty measures varied spectrally and with optical water type (Tables 4–7). For purposes of the ensuing discussion, the results are grouped into three broad categories — low chlorophyll open ocean (OWTs 1 and 2), mesotrophic to eutrophic open ocean (OWTs 3 and 4), and highly absorbing and scattering waters (OWTs 5, 6 and 7).

3.2.1. R_{rs} uncertainties in clear waters: optical water types 1 and 2

Open ocean waters represented by OWTs 1 and 2 are important as they encompass the largest oceanic areas (Fig. 1, Table 2). It is expected that they represent the best quality satellite R_{rs} since the MOBY vicarious calibration site is among these types. Results for these water types generally confirm this expectation (Tables 4–7, Fig. 4).

In these open ocean waters, RMSD patterns decrease progressively from the blue to red bands. SeaWiFS and MODIS-Aqua patterns are

Table 2
Distribution of matchup data by source across all optical water types (OWTs) for SeaWiFS and MODIS-Aqua. Also included is the percentage of global ocean area occupied by each OWT based on the SeaWiFS and MODIS climatologies.

OWT	N	%	N	%	N	%	N	%	N	%	%
SeaWIFS											
1	63	2.9	0	0.0	0	0.0	402	18.6	466	21.6	26.8
2	105	4.9	16	0.7	1	0.1	104	4.8	226	10.5	40.1
3	135	6.2	100	4.7	30	1.9	3	0.1	268	12.4	20.0
4	161	7.4	47	2.2	106	5.0	0	0.0	313	14.5	9.1
5	166	7.8	6	0.3	54	2.5	0	0.0	228	10.6	2.2
6	91	4.2	0	0.0	411	19.1	0	0.0	502	23.3	1.2
7	45	2.1	0	0.0	105	4.9	0	0.0	150	6.9	0.6
8	2	0.1	0	0.0	5	0.2	0	0.0	7	0.3	
Total	768	35.6	168	7.8	712	33.0	509	23.6	2159	100	100
MODIS-Aqua											
1	34	1.8	0	0.0	0	0.0	239	12.6	273	14.4	33.3
2	23	1.2	16	0.8	0	0.0	75	4.0	114	6.0	30.7
3	27	1.4	174	9.2	15	0.8	7	0.4	223	11.7	25.2
4	54	2.9	74	3.9	144	7.6	0	0.0	272	14.4	6.9
5	75	4.0	19	1.0	254	13.4	0	0.0	349	18.4	2.0
6	24	1.3	0	0.0	511	26.9	0	0.0	534	28.2	1.8
7	11	0.6	0	0.0	120	6.3	0	0.0	131	6.9	<0.05
8	1	0.1	0	0.0	6	0.3	0	0.0	7	0.4	
Total	249	13.1	283	14.9	1050	55.3	321	16.9	1903	100	100.0

similar, although MODIS-Aqua values are up to 20% higher in blue bands. The RMSD is dominated by the standard deviation (not shown), with a small contribution from the bias. Metrics based on the MOBY vicarious calibration data (dashed lines in Fig. 4) represent the optimally minimized uncertainty. These data were not included in the validation data used to calculate the other metrics.

The bias has a distinct zigzag pattern, which will be seen in other OWTs as well for both SeaWiFS and MODIS-Aqua. The bias (whether negative, zero, or positive) increases from 412 nm to 443 nm, then decreases from 443 nm to 490 nm, and generally increases again from 490 nm to either 510 (SeaWiFS) or 531 (MODIS-Aqua) nm before trending toward zero in the red bands at or near 670 nm.

MPD patterns (Table 6) are similar between the two sensors, with values ($\leq$7%) in the blue, increasing to slightly higher values in the green region (13%). The increased relative uncertainty in the red (50–60%) is due to the small R_{rs} signal at those wavelengths.

Table 3
Number of matchups for each OWT and spectral band for SeaWiFS and MODIS-Aqua. Also shown is the number of matchups used for the vicarious calibration (VC) and excluded from the analysis of uncertainty reported here.

	OWT	412	443	490	510	555	670
SeaWiFS	1	459	467	470	455	454	422
	2	203	224	227	201	192	156
	3	160	252	258	187	179	71
	4	236	291	307	146	223	107
	5	194	195	227	133	191	95
	6	499	414	507	80	468	101
	7	149	142	151	43	140	53
	8	7	7	7	2	7	2
	VC	143	143	143	143	143	143
		412	443	488	531	547	667
MODIS	1	241	247	247	225	219	230
	2	91	97	99	75	68	88
	3	78	170	186	24	13	138
	4	204	228	241	25	9	76
	5	350	226	369	42	15	51
	6	596	472	598	108	40	20
	7	156	137	157	38	20	12
	8	7	7	7	1	1	1
	VC	74	74	74	74	74	74

Relative uncertainty based on the MOBY vicarious calibration data meets the 5% goal in blue bands of both sensors. Interestingly, the OWT 1 results for MODIS-Aqua are only slightly higher than those of the vicarious calibration in all bands except the red band. The RPD values (Table 7) are higher than the MPD values, as expected from a positively skewed distribution.

3.2.2. R_{rs} uncertainties in mesotrophic/eutrophic waters: optical water types 3 and 4

While OWTs 3 and 4 occupy a smaller ocean area compared to OWTs 1 and 2, they are associated with important upwelling and productive zones around the globe including the Equatorial and North Atlantic regions (Fig. 1). Similar to OWTs 1 and 2, RMSD values for SeaWiFS progressively decrease from the blue to red bands (Fig. 5a, Table 4). Values at 412 nm are similar to those for OWTs 1 and 2, but values are more than 2 times higher at 555 nm and 670 nm. The RMSD for MODIS-Aqua (Fig. 5b) has a very different pattern, particularly in OWT 3 which has a much higher RMSD at 531 nm and 547 nm compared to the other bands. We believe this is a result of the small number of matchup points at those wavelengths (Table 3). Results based on fewer than 20 points are indicated by open symbols. The majority of data for OWTs 3 and 4 come from the BOUSSOLE mooring (Table 2) which lacks bands at 531 nm and 547 nm. Metrics derived by weighting the uncertainty statistics of all OWTs according to their global distribution in the satellite records are shown as red symbols and lines in Fig. 5.

Bias plays a small role in RMSD overall, as the standard deviation is nearly equal to RMSD. The zigzag feature is still present in both SeaWiFS and MODIS-Aqua, and except for the 443 nm bands, the bias is negative in all bands of both sensors. The large negative bias at 531 and 547 nm for MODIS-Aqua (Fig. 5d) contributes 11% and 22%, respectively, to the large RMSD in those bands. Elsewhere, the bias is generally only 2–3% of RMSD.

The MPD spectral patterns for SeaWiFS (Fig. 5e) are similar to those in OWTs 1 and 2, but with higher values in the blue and green regions. MODIS patterns are different in shape due to the lack of data for green bands (531 and 547 nm). MPD values for SeaWiFS range from 12 to 22% in the blue bands (412–443 nm), and 9 to 14% in the green bands (490–555 nm). Higher relative uncertainty is due in part to the smaller absolute magnitude of R_{rs} for these OWTs, compared to OWTs 1 and 2. RPD values (Table 7) are above MPD (Table 6), and generally higher for SeaWiFS than MODIS-Aqua. Like OWTs 1 and 2, the RPD and MPD are the highest at red bands with values exceeding 50% in some cases.

3.2.3. R_{rs} uncertainties in optically complex waters: optical water types 5, 6 and 7

OWTs 5 through 7 combined occupy the smallest ocean areas, and are associated with highly absorbing (OWT 5) and highly scattering (OWTs 6 and 7) conditions generally found in coastal regions. Collectively, they represent the traditional case 2 waters and are considered optically complex. Not surprisingly, they exhibit the highest values for all uncertainty measures as compared to OWTs 1 through 4 (Fig. 6). Values for RMSD are generally high in the blue and smaller in the red bands, but the patterns are flatter from blue to green and even increase for OWTs 6 and 7. Overall, RMSD values are lower for MODIS-Aqua compared to SeaWiFS for these types. Again, the small sample sizes account in part for the peaks at 531 and 547 nm (MODIS-Aqua), and open symbols indicate results based on fewer than 20 matchups.

The bias plays a somewhat larger role in RMSD for OWTs 5, 6 and 7 compared with other OWTs, particularly in the green bands where it represents 20–30% of the RMSD. A negative bias in OWT 5, largest at 412 nm for SeaWiFS, is present in all bands of both sensors.

The MPD spectral patterns exhibit a U-shape, with lower values in the green (10 to 20%) and higher values at the blue and red wavelengths.

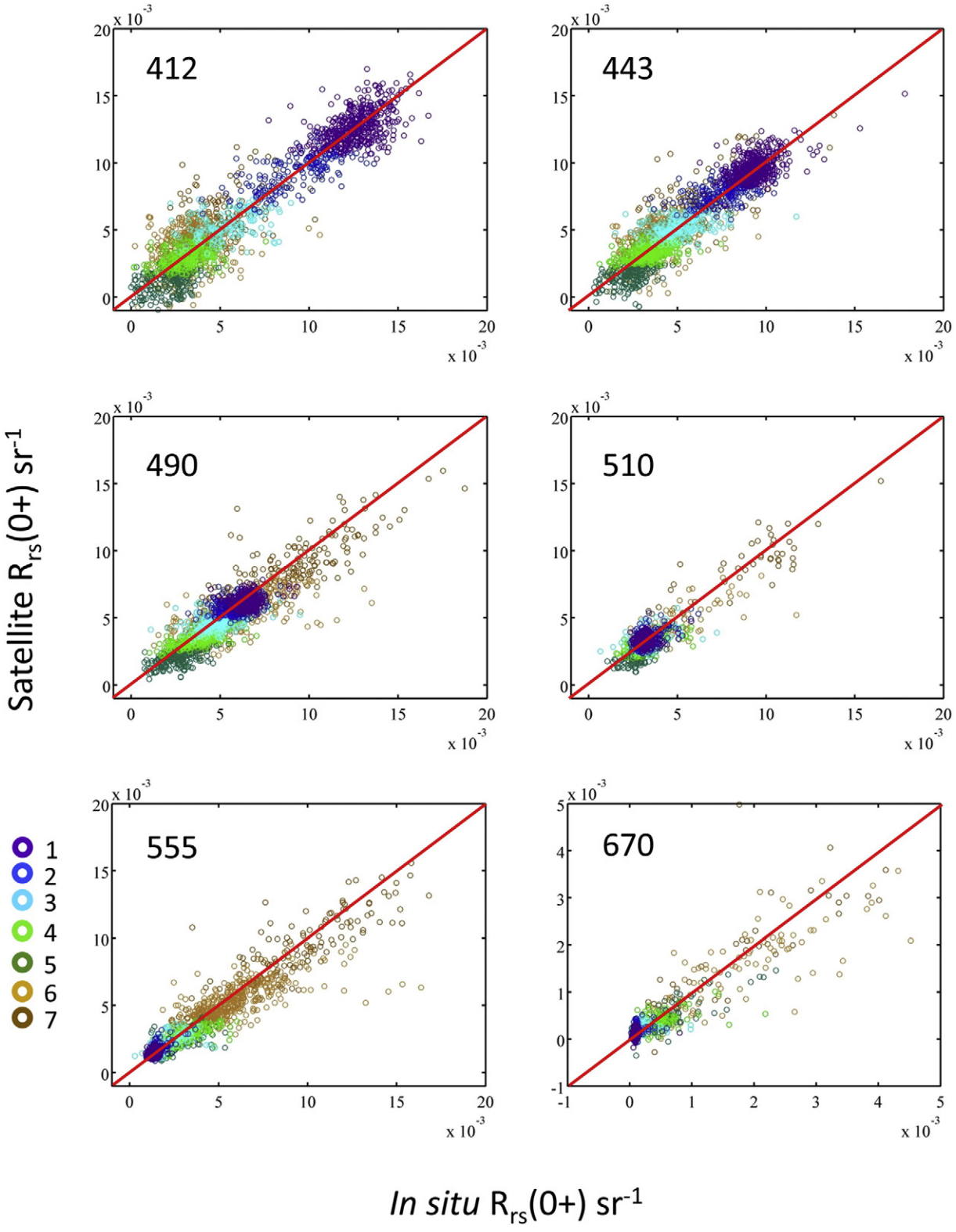

Fig. 2. Satellite vs. in situ $R_{rs}(0+)$ plots for SeaWiFS. Matchup points are color coded by OWT. Red line is 1:1.

MPD and RPD are the highest at 412 nm for OWT 5 with RPD exceeding 100% for both SeaWiFS and MODIS-Aqua (Table 7). Compared to the other OWTs, OWT 5 has the smallest R_{rs} magnitude at 412 nm, and consequently the size of its uncertainty relative to its magnitude is greatest at this wavelength. As in the case of other OWTs, the RPD values are higher than MPD values.

4. Discussion

4.1. Classification efficiency

Using a fuzzy classifier, we were able to distribute the uncertainty associated with each matchup pair among optical water types that

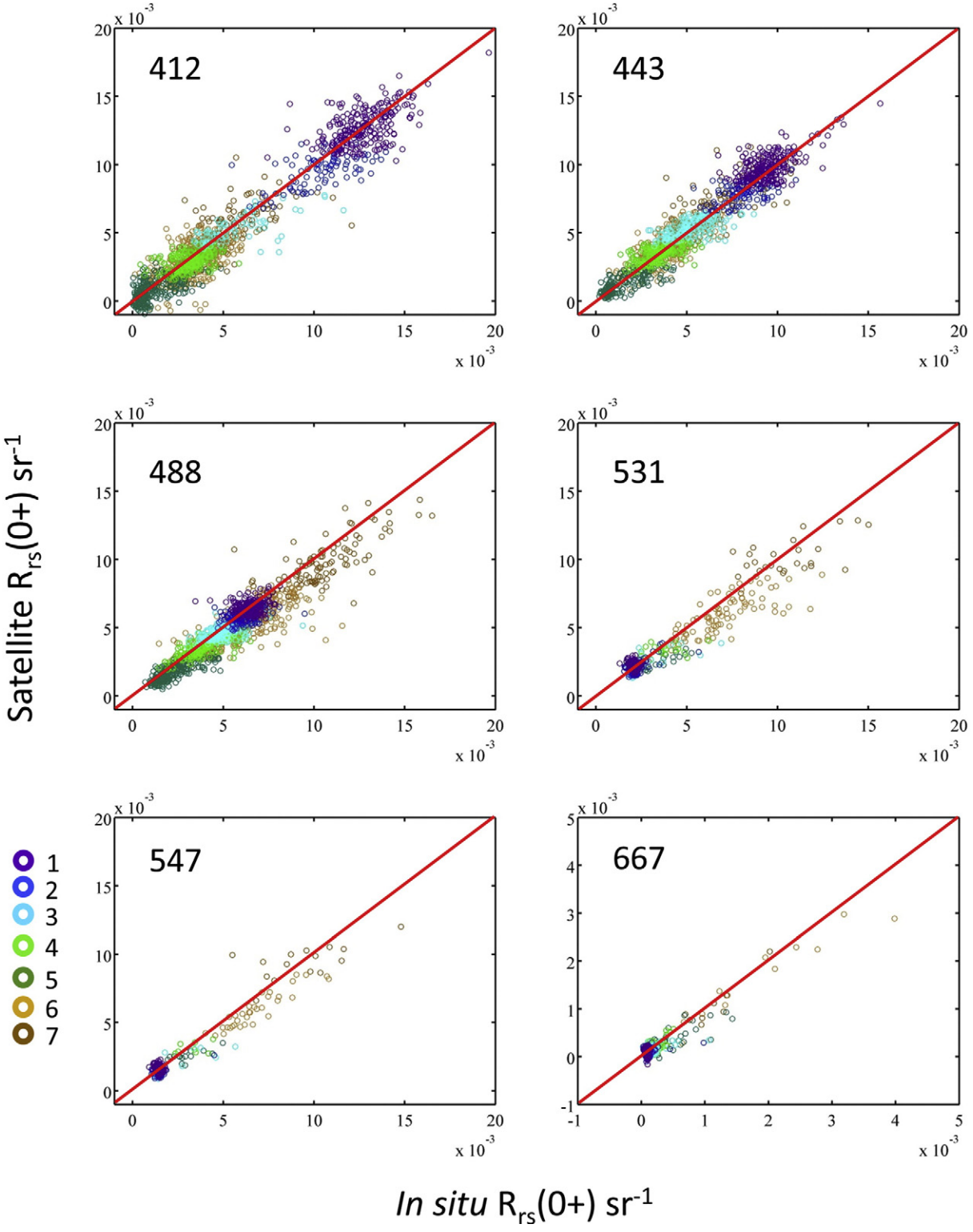

Fig. 3. Satellite vs. in situ $R_{rs}(0+)$ plots for MODIS-Aqua. Matchup points are color coded by OWT. Red line is 1:1.

have a similar spectral reflectance. This approach provided a mechanism to account for differences between open-ocean and coastal regions, and adjust for the uneven distribution of in situ data relative to the optical properties of the global ocean. In this study, satellite reflectances were used as input data to the classifier, rather than the in situ data for two reasons. First, not all bands were available for each matchup in situ datum compared to the satellite data. Secondly, in subsequent applications, reflectance uncertainty will be mapped using satellite data and fuzzy memberships to the optical water types.

4.2. Characteristics of radiance uncertainties

Published studies from the last 10 years report a range of uncertainty values for ocean color satellite radiances from 5 to 20% in the blue (or

Table 4
Spectral RMSD distribution by OWT for SeaWiFS and MODIS-Aqua. Also shown are the RMSD results weighted by the global area percentages and the results for the MOBY matchups used for vicarious calibration (VC). Units are sr^{-1}.

	OWT	412	443	490	510	555	670
SeaWiFS	1	0.00129	0.00100	0.00064	0.00043	0.00026	0.00009
	2	0.00138	0.00118	0.00085	0.00060	0.00041	0.00014
	3	0.00141	0.00113	0.00090	0.00067	0.00056	0.00018
	4	0.00105	0.00087	0.00081	0.00067	0.00070	0.00028
	5	0.00168	0.00117	0.00098	0.00083	0.00078	0.00031
	6	0.00169	0.00137	0.00123	0.00108	0.00113	0.00055
	7	0.00203	0.00174	0.00161	0.00140	0.00142	0.00046
	Global	0.00135	0.00110	0.00081	0.00059	0.00045	0.00016
	VC	0.00084	0.00062	0.00056	0.00029	0.00018	0.00006
		412	443	488	531	547	667
MODIS	1	0.00136	0.00111	0.00064	0.00034	0.00031	0.00007
	2	0.00166	0.00111	0.00079	0.00043	0.00033	0.00010
	3	0.00129	0.00088	0.00081	0.00122	0.00138	0.00014
	4	0.00096	0.00074	0.00075	0.00097	0.00079	0.00010
	5	0.00103	0.00081	0.00074	0.00127	0.00077	0.00027
	6	0.00137	0.00096	0.00120	0.00156	0.00108	0.00032
	7	0.00158	0.00145	0.00149	0.00149	0.00148	0.00021
	Global	0.00140	0.00102	0.00075	0.00068	0.00064	0.00011
	VC	0.00108	0.00076	0.00052	0.00028	0.00026	0.00006

more depending on wavelength) based on a variety of analysis methods, data sets, and geographic regions. Values based on data from deep open ocean waters lie at or near the desired 5% threshold (Bailey & Werdell, 2006; Hu et al., 2013) whereas matchups from areas closer to the continents are between 10 and 20% (Antoine et al., 2008; Melin, Zibordi, & Berthon, 2007). Bailey and Werdell (2006) further demonstrated a significant difference in uncertainties between open-ocean and coastal waters, representing case 1 and case 2 waters, respectively. Conversely, Melin et al. (2007) did not find any significant difference in uncertainties at the Venice Tower when matchup data were sorted by water type — in their case, 'case 1' and 'case 2' waters defined by the criteria set forth by Loisel and Morel (1998). However, this was based on a small data set at a specific location, whereas Bailey and Werdell (2006) used a larger, globally distributed data set. Maritorena, Fanton d'Andon, Mangin, and Siegel (2010) assessed radiance uncertainties on a combined matchup data set of ship and buoy (BOUSSOLE) and found MPD to range between 12 and 20% for the visible channels of SeaWiFS and MODIS-Aqua.

In this study, we pooled the geographically dispersed matchup data sets used in earlier studies into large, comprehensive matchup data sets for a unified analysis. The in situ data were obtained from fixed sites with long temporal coverage (MOBY, BOUSSOLE, and Aeronet-OC sites including the Venice Tower) and combined with distributed ship data from various locations around the global oceans over the mission periods of SeaWiFS (1997–2010) and MODIS-Aqua (2002–2012). Analysis of data subsets sorted by objective criteria can reveal patterns that would otherwise be obscured in large, aggregate collections. For our approach, we set out to characterize the uncertainties for satellite-derived remote-sensing reflectance according to optical water type classification. This approach is attractive because it provides 1) an objective means to group data based on a common set of spectral reflectances which are independent of geographic location and satellite sensor, and 2) an avenue for pixel-by-pixel mapping of uncertainty metrics for ocean color imagery.

Our results show that the main descriptors of uncertainty for satellite reflectance – RMSD, standard deviation, bias, and relative uncertainty measures – exhibit water-type dependencies in both spectral pattern and magnitude. RMSD – the most comprehensive uncertainty measure – generally decreases across wavelengths from blue to red regardless of optical water type. The RMSD magnitude increases from clear waters to turbid waters, for all wavelengths, but more significantly for case 2 waters that have high scattering properties. The biases varied by OWT in magnitude, but a persistent zigzag pattern was repeated across all OWTs.

Table 5
Spectral bias distribution by OWT for SeaWiFS and MODIS-Aqua. Also shown are the bias results weighted by the global area percentages and the results for the MOBY matchups used for vicarious calibration (VC). Units are sr^{-1}.

	OWT	412	443	490	510	555	670
SeaWiFS	1	0.00020	0.00033	−0.00021	0.00010	0.00010	0.00002
	2	0.00011	0.00033	0.00001	0.00014	0.00017	0.00006
	3	−0.00002	0.00011	−0.00019	−0.00008	−0.00006	−0.00001
	4	−0.00018	−0.00010	−0.00037	−0.00029	−0.00033	−0.00007
	5	−0.00119	−0.00077	−0.00066	−0.00063	−0.00048	−0.00018
	6	0.00012	0.00026	−0.00037	−0.00021	−0.00037	−0.00021
	7	0.00069	0.00076	−0.00027	−0.00015	−0.00030	−0.00009
	Global	0.00006	0.00022	−0.00014	0.00002	0.00004	0.00001
	VC	−0.00018	0.00013	−0.00039	0.00003	0.00004	0.00001
		412	443	488	531	547	667
MODIS	1	0.00016	0.00047	0.00009	0.00015	0.00018	0.00001
	2	−0.00075	−0.00019	−0.00028	−0.00014	−0.00006	−0.00002
	3	−0.00027	0.00018	−0.00022	−0.00056	−0.00087	−0.00003
	4	−0.00023	0.00002	−0.00037	−0.00041	−0.00028	0.00001
	5	−0.00052	−0.00030	−0.00049	−0.00086	−0.00047	−0.00014
	6	−0.00058	−0.00010	−0.00074	−0.00108	−0.00078	−0.00012
	7	−0.00021	0.00037	−0.00071	−0.00020	−0.00009	−0.00009
	Global	−0.00028	0.00014	−0.00017	−0.00020	−0.00022	−0.00002
	VC	−0.00016	0.00014	−0.00009	0.00008	0.00013	0.00000

Table 6
Spectral MPD distribution by OWT for SeaWiFS and MODIS-Aqua. Also shown are the MPD results weighted by the global area percentages and the results for the MOBY matchups used for vicarious calibration (VC). Units are %.

	OWT	412	443	490	510	555	670
SeaWiFS	1	6.1	6.7	7.0	8.7	13.0	50.7
	2	8.1	9.6	10.0	10.1	13.2	56.7
	3	14.7	12.3	9.1	9.6	13.3	51.3
	4	22.3	16.4	13.8	13.4	13.8	35.0
	5	63.2	37.5	26.0	23.2	21.3	31.5
	6	31.3	24.0	13.7	17.3	12.5	23.5
	7	20.9	16.7	10.8	9.6	10.1	18.8
	Global	11.8	10.8	9.8	10.3	13.4	50.8
	VC	4.0	4.3	6.9	5.2	7.9	38.5
		412	443	488	531	547	667
MODIS	1	5.8	7.0	5.4	10.0	13.1	42.8
	2	10.5	8.5	8.8	12.1	14.1	51.6
	3	9.5	10.2	7.5	16.8	32.2	31.1
	4	17.5	12.0	12.2	15.1	16.8	40.1
	5	60.0	32.9	21.2	25.6	18.2	39.6
	6	19.6	12.5	12.2	15.5	11.1	8.0
	7	16.9	10.2	7.9	10.8	6.2	20.8
	Global	10.4	9.2	7.9	13.1	18.5	41.6
	VC	5.2	5.8	5.1	9.1	12.4	28.6

The relative uncertainty measures – RPD and MDP – show the greatest dependency on water type. The emphasis on relative uncertainty assumes that errors are proportional to the signal. To a large extent, this is true when the signal is high, but evidently there is a residual error that does not scale with the radiance signal. In terms of relative uncertainty, the impacts of a residual error are more pronounced in water types with low absolute radiances (at any spectral band). For example, OWT 5 has extremely high relative uncertainty in the blue bands where strong absorption makes the signal low. This impact is also seen in the red bands, which have low signal magnitudes due to strong water absorption.

The desired goal of reaching 5% relative uncertainty in the blue part of the spectrum for open ocean waters remains elusive, although MPD values are at or below 7% (Table 6). In contrast, water types typically found near coastal environments (OWTs 5 through 7) show a much higher MPD and RPD, as well as high RMSD. However, even if RMSD were reduced to the same level as that of the open ocean, the MPD would only be reduced to between 10 and 20% in the blue bands. It likely will never be reduced to 5% in these environments unless the residual errors (possibly due to noise or calibration errors) are removed or reduced.

Table 7
Spectral RPD distribution by OWT for SeaWiFS and MODIS-Aqua. Also shown are the RPD results weighted by the global area percentages and the results for the MOBY matchups used for vicarious calibration (VC). Units are %.

	OWT	412	443	490	510	555	670
SeaWiFS	1	7.8	8.4	7.9	10.6	15.5	66.9
	2	12.3	13.3	12.0	13.9	20.1	99.3
	3	22.5	18.3	14.6	15.7	20.5	70.7
	4	42.5	23.1	16.5	16.2	16.9	57.1
	5	258.3	43.8	29.3	26.0	24.0	41.0
	6	52.8	32.1	19.1	20.1	16.0	30.3
	7	33.9	24.8	15.2	14.2	13.6	31.1
	Global	22.0	14.9	12.3	13.9	18.6	78.5
	VC	5.3	5.4	7.4	7.2	10.5	44.9
		412	443	488	531	547	667
MODIS	1	8.5	9.1	7.9	13.0	17.5	62.6
	2	12.4	10.1	10.1	13.5	15.7	64.5
	3	14.2	13.9	10.1	21.0	31.5	48.1
	4	30.7	17.9	13.5	19.3	19.5	54.3
	5	135.2	41.8	23.2	23.8	18.5	47.9
	6	33.7	18.5	15.5	16.2	12.5	14.6
	7	22.3	15.5	10.4	12.3	11.5	20.9
	Global	15.7	12.1	10.0	15.9	20.5	57.6
	VC	6.8	6.5	6.6	10.9	14.8	45.4

4.3. Sources of R_{rs} uncertainties

The goal of validation analysis is to assess the performance of satellite data based on matchup data sets. This type of analysis has three sources of uncertainty: one from each data source (in this case, the in situ radiometer and the satellite measurement), and the third from the imprecision in the matchup itself (time/space differences, as well as differences in the spectral band widths and exact center channel location). In principle, these three sources of error should be independent. Therefore, non-satellite sources can be estimated separately and deducted from the total uncertainty to arrive at the satellite uncertainty. Hooker and Maritorena (2000) estimated a 3–5% uncertainty for in situ radiometers when strict protocols are rigorously followed, and Antoine et al. (2008) estimated that the radiometer at BOUSSOLE has a 6% uncertainty after accounting for additional sources of uncertainty beyond 3% for the radiometer itself. Bailey and Werdell (2006) deducted 5% for uncertainties attributed to in situ sensors, with the remainder assigned to satellite sources (i.e., calibration and atmospheric correction errors).

The time/space mismatch is an inherent source of uncertainty for matchup data sets, and consequently there is a need to set boundary criteria for qualifying matched points as valid. In this study, the criteria were set to plus/minus three-hour time differential between satellite overpass and in situ measurement, and the footprint size was centered on a 5×5 pixel box around the in situ point location. In addition, at least 50% of the pixels within that box had to be valid processed pixels and have a median coefficient of variation less than 0.15.

Such differences are impacted by the nature of the environment around the matchup point that depends on water movement and natural optical changes within the water itself. To assess heterogeneity in the vicinity of our matchup points we examined the median values of the CV for each OWT (Table 8). While all values are under the 0.15 threshold, the increasing median CV value with OWT is indicative of increasing heterogeneity. Progressing from OWT 1 to OWT 7, there is a general increase in chlorophyll concentration and/or optical complexity. The increase in CV with ascending OWT indicates a larger contribution to uncertainty from the matchup imprecision as environments become more eutrophic or closer to land. For OWTs 1 through 4 the mismatch may not be a significant issue, as one would expect space and time scales of variability to be larger in the open ocean.

We varied the threshold of the CV criteria in the SeaBASS option menu between 0.05 and 0.6, and found that above 0.15 (the default value) there was negligible impact on the metrics, indicating that the default value is already at a high threshold. As CV was reduced from 0.15 to 0.05, the total number of matchup points was reduced from 2166 to 1434 for SeaWiFS, and from 1903 to 1195 for MODIS-Aqua. RMSD values decreased from 1 to 10% for the blue wavelengths and up to 30% for green wavelengths across OWTs for both SeaWiFS and MODIS-Aqua. However, in some cases, RMSD showed the opposite trend and increased by a few percent. A similar analysis was conducted by Melin et al. (2007). When they tightened time and space criteria for matchup selection, less than a 2% change resulted in their uncertainty estimates using RPD, suggesting that spatial mismatch issues are minimal at the Venice Tower, which is a coastal site.

One approach to minimize the pitfalls of matchup analysis is simply to avoid it, and use alternate methods such as satellite-to-satellite comparisons (e.g., Hu et al., 2013; Melin, 2010). This type of approach is based on complete spectra and large numbers of matchups, but it does not resolve biases in the satellite radiances, and therefore sets a lower limit for uncertainty. In the end, there is no practical way of quantifying the *error* – defined as the difference between a measurement and its true value (Taylor, 1982) – in satellite products from matchup or other analysis. All methods contain limitations, and thus an ensemble strategy remains the most comprehensive way to understand the

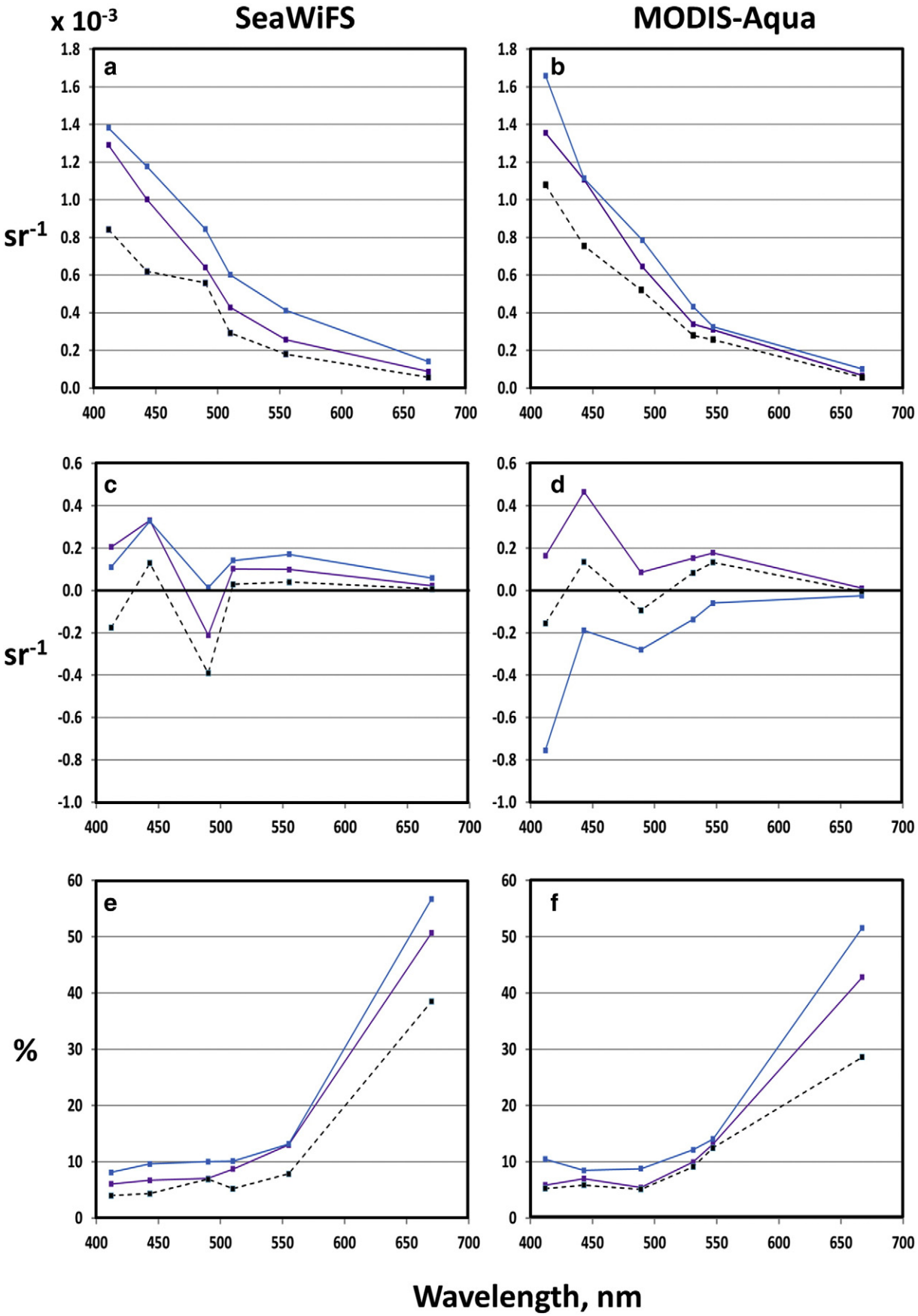

Fig. 4. Spectral R_{rs} uncertainty measures for OWT 1 (purple) and OWT 2 (blue). a, b: RMSD; c, d: bias; e, f: MPD. Dashed lines are based on the MOBY data used for vicarious calibration. SeaWiFS (left panels) and MODIS-Aqua (right panels).

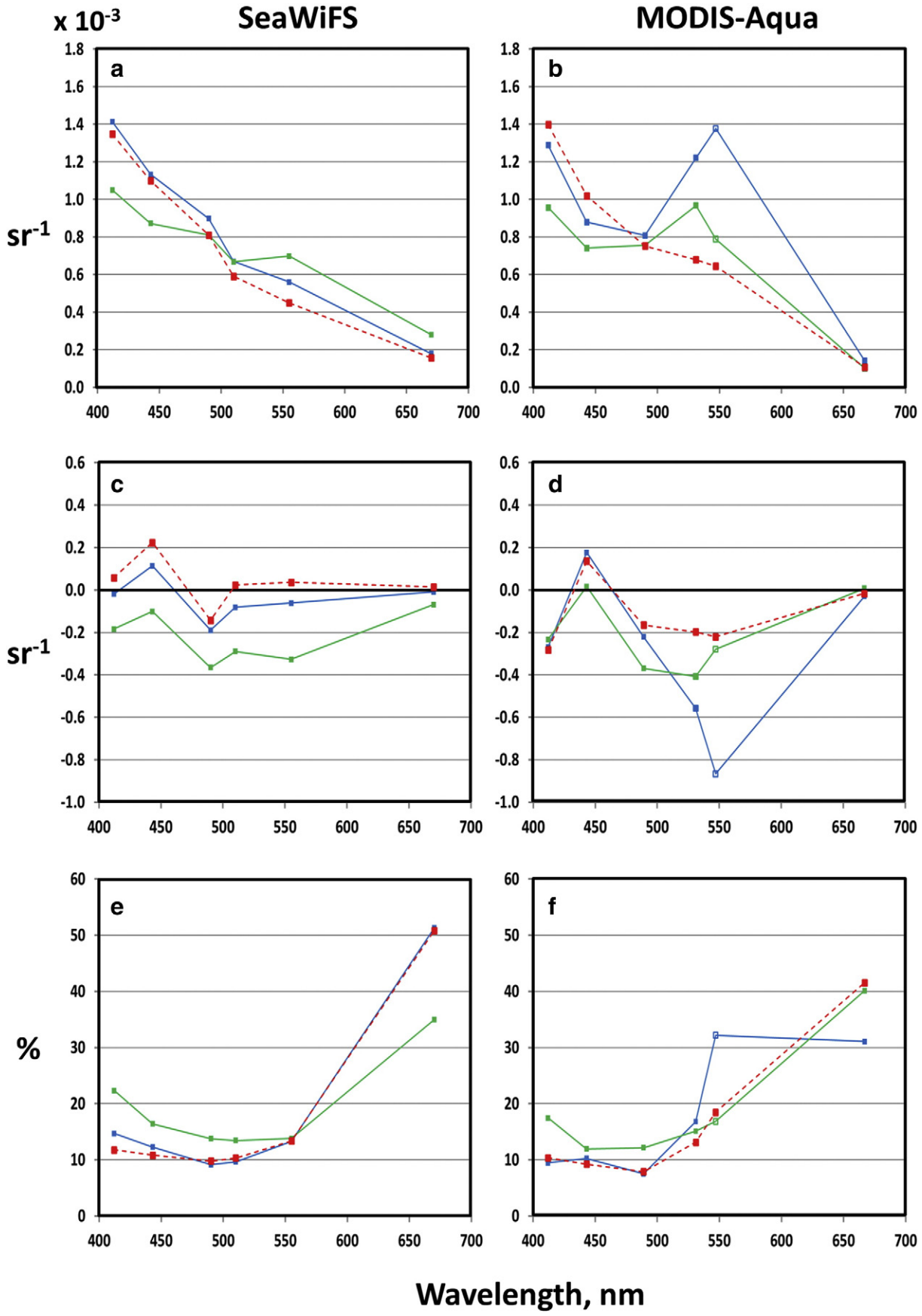

Fig. 5. Spectral R_{rs} uncertainty measures for OWT 3 (blue) and OWT 4 (green). Global uncertainty measures based on all OWTs weighted by the global area percentages are shown in red. a, b: RMSD; c, d: bias; e, f: MPD. Results based on fewer than 20 points are indicated by open symbols and dashed lines. SeaWiFS (left panels) and MODIS-Aqua (right panels).

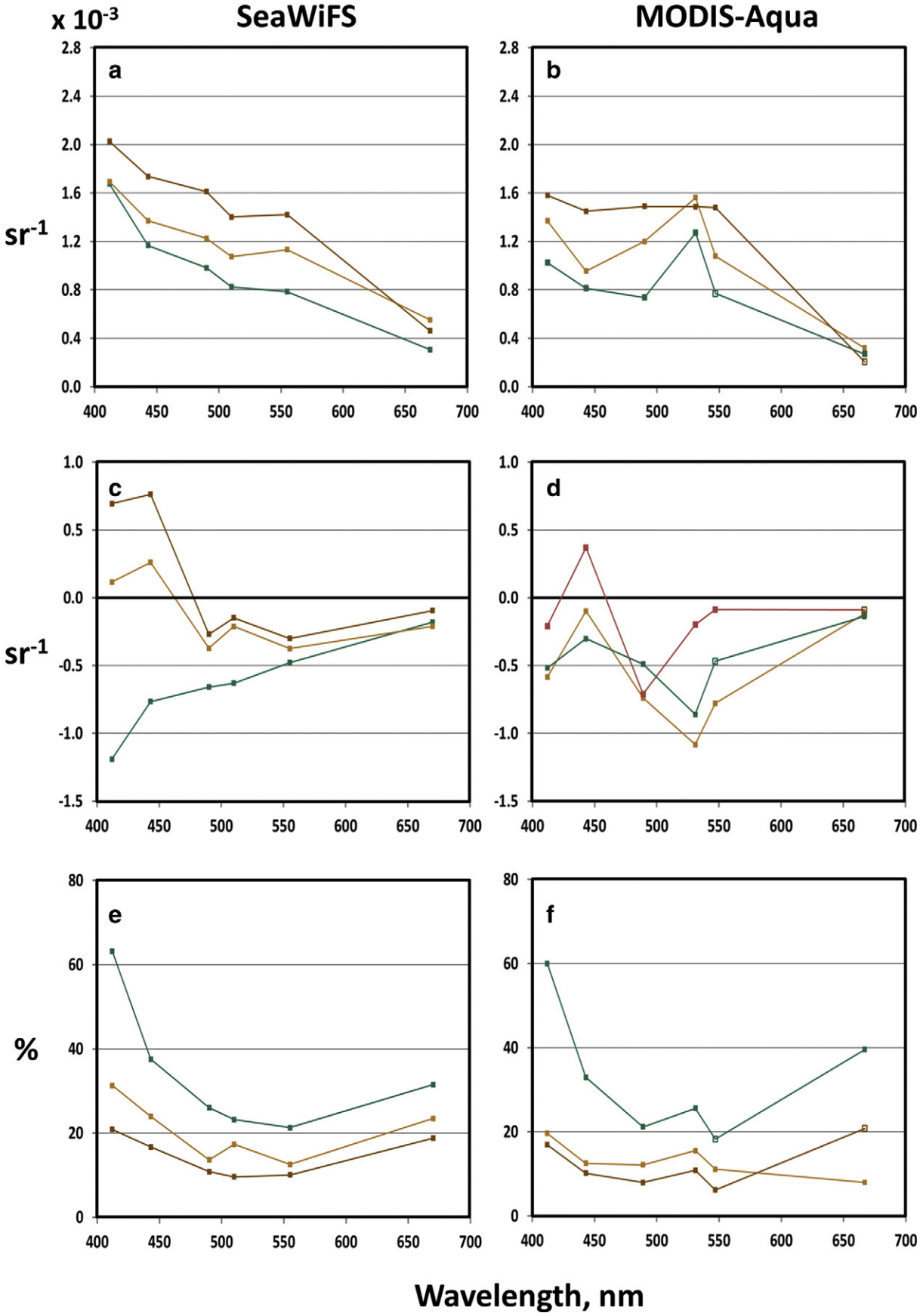

Fig. 6. Spectral R_{rs} uncertainty measures for OWT 5 (dark green), OWT 6 (tan) and 7 (brown). a, b: RMSD; c, d: bias; e, f: MPD. Results based on fewer than 20 points are indicated by open symbols and dashed lines. SeaWiFS (left panels) and MODIS-Aqua (right panels).

Table 8
Median values of the coefficient of variation within the 5 × 5 pixel box of extracted satellite reflectances (a threshold of CV < 0.15 was used to accept a matchup data point).

OWT	SeaWiFS	MODIS-Aqua
1	0.0213	0.0139
2	0.0282	0.0200
3	0.0273	0.0185
4	0.0353	0.0415
5	0.0495	0.0508
6	0.0671	0.0623
7	0.0545	0.0626

performance of satellite products. While the comparisons between satellite and in situ matchup data are subject to mismatch issues and not pure product errors, they remain a necessary and important means of verifying satellite products, and represent a maximum level of uncertainty that includes satellite, in situ, and matchup uncertainties (e.g., point-to-pixel scaling and time gaps).

The uncertainty sources for satellite radiances stem from the calibration of the sensors, including the vicarious calibration conducted on orbit, out-of-band correction factors, and the atmospheric correction algorithm used in deriving water-leaving radiance from TOA radiance. Errors in the calibration would impact all imagery from the same sensor. Although biases, in part minimized by vicarious calibration, make a smaller contribution than the standard deviation for all OWTs, they are of practical concern because they are not removed when data are averaged, for example, in the creation of level-3 products. We examined whether the biases computed for this analysis are non-zero based on a threshold of $\pm 0.0002\ sr^{-1}$, which Hu et al. (2013) used as equivalent to a zero bias. If this range is taken, the biases for SeaWiFS OWTs 1 through 3 are within this threshold for all spectral bands except one (443 nm for OWTs 1 and 2). Biases are predominantly 'non-zero' for OWTs 4 through 7 over the blue and green bands for both SeaWiFS and MODIS-Aqua. It is beyond the scope of this study to quantify the impact of all potential error sources on the quality of the satellite remote sensing reflectance. However, we further consider the sources of bias in the 'case 2' OWTs 5, 6 and 7.

OWT 5 – a type associated with highly absorbing waters typically found near coasts – shows a negative bias across all wavelengths which is most pronounced in the blue bands for both sensors. A well-known cause of negative biases in coastal regions is the improper modeling of aerosols (Gordon, 1997). A non-zero contribution of water-leaving radiance in the NIR bands, violating the black-pixel assumption (Bailey et al., 2010), results in an over-estimation of the aerosol optical thickness and thus an under-estimation of the water-leaving radiance. In this case, the resulting negative bias error would increase towards lower wavelengths because of the extrapolation from aerosol (NIR) bands. The presence of light-absorbing aerosols, another atmospheric feature found above coastal areas, could also contribute to negative biases in water-leaving radiances.

OWTs 6 and 7 – highly scattering waters typically found in coastal regions – also show negative biases at wavelengths greater than 443 nm. It is unclear why these water types show positive biases in blue wavelength bands at 412 and 443 nm, as these waters would be subject to the same over-correction effects with increasing negative bias towards the blue bands. The iterative atmospheric correction scheme presented in Bailey et al. (2010) was designed to account for non-zero water-leaving radiance in the NIR, and they reported a significant reduction in negative water leaving radiance retrievals. However, they note that the approach cannot correct for all turbid water conditions, and has problems in waters where the empirical backscattering model was not developed. Whatever the causes, accuracy issues impacting coastal waters are a function of the atmospheric and in-water composition, especially in the NIR where algorithm assumptions drive the corrections for the remaining visible bands.

Recent atmospheric correction algorithms have been developed specifically addressing the issues of the NIR problem in coastal waters (e.g., Ruddick, De Cauwer, & Park, 2006; Schroeder, Behnert, Schaale, Fischer, & Doerffer, 2007; Stumpf, Arnone, Gould, Martinolich, & Ransibrahmanakul, 2003; Wang, Son, & Shi, 2009). Goyens, Jamet, and Schroeder (2013) examined different atmospheric correction schemes for turbid, coastal waters and found varying levels of performance when viewed from a water-type perspective, suggesting that optical water types were differentially resolved with different schemes, at least in these turbid coastal waters. At present, a scheme that blends the default open-ocean atmospheric correction algorithm with coastal-oriented algorithms in a unified framework is not yet operational at the agency level. Advances are also being made in algorithms that account for absorbing aerosols (e.g., Brajard, Moulin, & Thiria, 2008; Shi & Wang, 2007). It is expected that biases due to these two sources will be reduced when atmospheric correction algorithms become more mature, and these can be applied retroactively to both SeaWiFS and MODIS-Aqua data sets which should improve the quality of radiance products in all water types.

Another potential error source is the bi-directional correction factors (f/Q) applied during atmospheric correction. Bi-directional effects arise from the non-isotropic nature of radiances exiting a water body, and depend on illumination/viewing geometry and inherent optical properties of the water body (Morel et al., 2002). These effects cannot be ignored and must be dealt with during atmospheric correction. Currently, these are accessed in the codes in a lookup table as a function of chlorophyll concentration. Thus, any error in the satellite-derived chlorophyll concentration would impact the bi-directional correction. Melin et al. (2007) analyzed the impacts of using algorithm-based chlorophyll values versus in situ values, and found relative differences at 555 nm ranging from −4.1% to +2.3%, which are large enough to make an impact. Furthermore, Loisel and Morel (2001) showed that the f/Q factors are not constant but vary as a function of water type, and this would have a differential impact on the OWT-specific results in this study. However, it is outside of the scope of the present study to examine how these effects might impact radiances in different water types, as it would require coincident chlorophyll measurements at a minimum.

5. Conclusions

This study examined the quality of remote sensing reflectances from two NASA satellite ocean color sensors – SeaWiFS and MODIS-Aqua – based on matchup analyses. The in situ data sets used for the analyses were an assemblage of ship, buoy and platform data that have been previously analyzed though not collectively.

Application of a fuzzy classifier allowed for the partitioning of uncertainty among optical water types. By characterizing uncertainties for the different optical water types, we have provided the metrics needed to produce uncertainty fields for satellite remote-sensing reflectance products. Specifically, fuzzy memberships can be determined and used to weight OWT uncertainty measures to arrive at the distributed uncertainty fields for any SeaWiFS or MODIS-Aqua image.

The desired goal of 5% accuracy for water-leaving radiance in blue bands for the open ocean has yet to be achieved, although the MPD for SeaWiFS and MODIS-Aqua (≤7% in blue bands) is approaching that goal. This finding supports the value of assessing satellite ocean color uncertainty in the context of the distribution of in-water optical properties found globally, and is consistent with the findings of Hu et al. (2013).

The 5% MPD goal is unlikely to ever be achieved for water types outside of the open ocean. The uncertainties are higher for coastal waters where absorption and scattering processes become more extreme. While these water types are a fraction of the total ocean surface area, they are important regions that are receiving increased focus for satellite ocean color applications to monitor coastal and lake processes. These results reveal that radiance uncertainty for these water types is

greater than for the open ocean, and stands to benefit from targeted improvements to the atmospheric correction. However, reduction of the RMSD to open ocean levels will, at best, only lead to 10–20% MPD uncertainty.

Acknowledgments

We are grateful to the NASA's Ocean Biology Processing Group for maintaining the SeaBASS data archive and creating the web interface used to assemble validation data sets. Specifically, we thank Sean Bailey, Bryan Franz, Chris Procter, and Jeremy Werdell for their assistance in acquiring and interpreting the data. We'd also like to thank the many contributors to SeaBASS, without whom this work would not be possible. We are grateful to Brent Holben and Giuseppe Zibordi for their leadership and personal commitment in creating, expanding and maintaining the AERONET-OC network. We also wish to thank the following individual AERONET-OC contributors to SeaBASS: G. Zibordi for providing data from the Venice, Abu Al Bukhoosh, Gloria, Gustav Dalen, and Helsinki Lighthouse sites; B. Holben for data from the COVE site; Sam Ahmed and Alex Gilerson for data from the LISCO site; Thomas Schroeder for data from the Lucinda site; Susanne Kratzer for data from the Palgrunden site; and Alan Weidemann for data from the WaveCIS site. We are grateful to David Antoine for providing the BOUSSOLE data set to SeaBASS. Community sharing and access to these data sets are critical for evaluating and developing bio-optical algorithms and products for ocean color missions. Finally, we'd like to thank the three anonymous reviewers whose constructive comments have improved the manuscript. This work was funded by the NASA grant NNX11AL20G.

References

Antoine, D., d'Ortenzio, F., Hooker, S.B., Becu, G., Gentili, B., Tailliez, D., et al. (2008). Assessment of uncertainty in the ocean reflectance determined by three satellite ocean color sensors (MERIS, SeaWiFS and MODIS-A) at an offshore site in the Mediterranean Sea (BOUSSOLE project). *Journal of Geophysical Research*, *113*. http://dx.doi.org/10.1029/2007JC004472.

Aurin, D.A., Mannino, A., & Franz, B.A. (2013). Spatially resolving ocean color and sediment dispersion in river plumes, coastal systems, and continental shelf waters. *Remote Sensing of Environment*, *137*, 212–225.

Bailey, S.W., Franz, B.A., & Werdell, P.J. (2010). Estimation of near-infrared water-leaving reflectance for satellite ocean color data processing. *Optics Express*, *18*, 7521–7527.

Bailey, S.W., Hooker, S.B., Antoine, D., Franz, B.A., & Werdell, P.J. (2008). Sources and assumptions for the vicarious calibration of ocean color satellite observations. *Applied Optics*, *47*, 2035–2045.

Bailey, S.W., & Werdell, P.J. (2006). A multi-sensor approach for the on-orbit validation of ocean color satellite data products. *Remote Sensing of Environment*, *102*, 12–23.

Barnes, R.A., Clark, D.A., Esaias, W.E., Fargion, G.S., Feldman, G.C., & McClain, C.R. (2003). Development of a consistent multi-sensor global ocean colour time series. *International Journal of Remote Sensing*, *24*, 4047–4064.

Brajard, J., Moulin, C., & Thiria, S. (2008). Atmospheric correction of SeaWiFS ocean color imagery in the presence of absorbing aerosols off the Indian coast using a neuro-variational method. *Geophysical Research Letters*, *35*. http://dx.doi.org/10.1029/2008GL035179.

Clark, D.K., Feinholz, M., Yarbrough, M., Johnson, B.C., Brown, S.W., Kim, Y.S., et al. (2002). Overview of the radiometric calibration of MOBY. In W.L. Barnes (Ed.), *Earth observing systems VI, vol. 4483*. (pp. 64–76) (SPIE).

Clark, D.K., Yarbrough, M., Feinholz, M., Flora, S., Broenkow, W., Kim, Y.S., et al. (2003). MOBY, a radiometric buoy for performance monitoring and vicarious calibration of satellite ocean color sensors: Measurement and data analysis protocols. In J.L. Mueller, G.S. Gargion, & C.R. McClain (Eds.), *Ocean optics protocols for satellite ocean color sensor validation, NASA Tech. Memo. 2003-211621/Rev.4, VI*, Greenbelt, MD: NASA GSFC (139 pp.).

Franz, B.A., Bailey, S.W., Werdell, P.J., & McClain, C.R. (2007). Sensor-independent approach to the vicarious calibration of satellite ocean color radiometry. *Applied Optics*, *46*, 5068–5082.

Gordon, H.R. (1997). Atmospheric correction of ocean color imagery in the Earth Observing System era. *Journal of Geophysical Research*, *102*(14), 17,081–17,106.

Goyens, C., Jamet, C., & Schroeder, T. (2013). Evaluation of four atmospheric correction algorithms for MODIS-Aqua imagery over contrasted coastal waters. *Remote Sensing of Environment*, *131*, 63–75.

Holben, B. N., Eck, T. F., Slutsker, I., Tanre, D., Buis, J. P., & Setzer, A. (1998). AERONET — a federated instrument network and data archive for aerosol characterization. *Remote Sensing of Environment*, *66*, 1–16.

Hooker, S.B., Esaias, W.E., Feldman, G.C., Gregg, W.W., & McClain, C.R. (1992). *An overview of SeaWiFS and ocean color. NASA Tech. Memo., vol. 104566*, Greenbelt, MD: National Aeronautics and Space Administration, Goddard Space Flight Center.

Hooker, S.B., & Maritorena, S. (2000). An evaluation of oceanographic radiometers and deployment methodologies. *Journal of Atmospheric and Oceanic Technology*, *17*(6), 811–830.

Hu, C., & Campbell, J. (2014). Oceanic chlorophyll-a content. In J.M. Hanes (Ed.), *Biophysical applications of satellite remote sensing*. Springer Remote Sensing/Photogrammetry. http://dx.doi.org/10.1007/978-3-642-25047-7_7, 171-203.

Hu, C., Feng, L., & Lee, Z. (2013). Uncertainties of SeaWiFS and MODIS remote sensing reflectance: Implications from clear water measurements. *Remote Sensing of Environment*, *76*, 239–249.

Loisel, H., & Morel, A. (1998). Light scattering and chlorophyll concentration in case 1 waters: A reexamination. *Limnology and Oceanography*, *43*, 847–858.

Loisel, H., & Morel, A. (2001). Non-isotropy of the upward radiance field in typical coastal (Case 2) waters: A reexamination. *International Journal of Remote Sensing*, *22*, 275–295.

Maritorena, S., Fanton d'Andon, O.H., Mangin, A., & Siegel, D. (2010). Consistent merging of satellite ocean color data sets using a bio-optical model. *Remote Sensing of Environment*, *114*, 1791–1804.

Maritorena, S., & Siegel, D. (2005). Consistent merging of satellite ocean color data sets using a bio-optical model. *Remote Sensing of Environment*, *94*, 429–440.

Melin, F. (2010). Global distribution of the random uncertainty associated with satellite-derived Chla. *IEEE Geoscience and Remote Sensing Letters*, *7*(1), 220–224.

Melin, F., Zibordi, G., & Berthon, J. -F. (2007). Assessment of satellite ocean color products at a coastal site. *Remote Sensing of Environment*, *110*, 192–215.

Melin, F., Zibordi, G., & Djavidnia, S. (2009). Merged series of normalized water leaving radiances obtained from multiple satellite missions for the Mediterranean Sea. *Advances in Space Research*, *43*(3), 423–437.

Moore, T.S., Campbell, J.W., & Dowell, M.D. (2009). A class-based approach to characterizing and mapping the uncertainty of the MODIS ocean chlorophyll product. *Remote Sensing of the Environment*, *113*, 2424–2430.

Morel, A., Antoine, D., & Gentili, B. (2002). Bidirectional reflectance of oceanic waters: Accounting for Raman emission and varying particle scattering phase function. *Applied Optics*, *41*, 6289–6306.

National Research Council (2011). *Assessing requirements for sustained ocean color research and operations*. Washington, DC: National Academic Press.

Ruddick, K.G., De Cauwer, V., & Park, Y. -J. (2006). Seaborne measurements of near infrared water-leaving reflectance: The similarity spectrum for turbid waters. *Limnology and Oceanography*, *51*, 1167–1179.

Schroeder, T., Behnert, I., Schaale, M., Fischer, J., & Doerffer, R. (2007). Atmospheric correction algorithm for MERIS above case-2 waters. *International Journal of Remote Sensing*, *28*, 1469–1486.

Shi, W., & Wang, M. (2007). Detection of turbid waters and absorbing aerosols for the MODIS ocean color data processing. *Remote Sensing of Environment*, *110*, 149–161.

Siegel, D.A., Wang, M., Maritorena, S., & Robinson, W. (2000). Atmospheric correction of satellite ocean color imagery: The black pixel assumption. *Applied Optics*, *39*, 3582–3591.

Stumpf, R.P., Arnone, R.A., Gould, R.W., Martinolich, P.M., & Ransibrahmanakul, V. (2003). A partially coupled ocean–atmosphere model retrieval of water-leaving radiance from SeaWiFS in coastal waters. *SeaWiFS postlaunch technical report series, volume 22: algorithm updates for the fourth SeaWiFS data reprocessing. NASA Technical Memorandum 2003-206892*.

Szeto, M., Campbell, J.W., Moore, T.S., & Werdell, P.J. (2011). Are the world's oceans optically different? *Journal of Geophysical Research*. http://dx.doi.org/10.1029/2011JC007230.

Taylor, J.R. (1982). *An introduction to error analysis*. Sausalito, CA: University Science Books.

Wang, M., Son, S., & Shi, W. (2009). Evaluation of MODIS SWIR and NIR-SWIR atmospheric correction algorithms using SeaBASS data. *Remote Sensing of Environment*, *113*, 635–644.

Werdell, P.J., & Bailey, S.W. (2005). An improved bio-optical data set for ocean color algorithm development and satellite data product validation. *Remote Sensing of Environment*, *98*(1), 122–140.

Werdell, P.J., Bailey, S.W., Fargion, G.S., Pietras, C., Knobelspiesse, K.D., Feldman, G.C., et al. (2003). Unique data repository facilitates ocean color satellite validation. *EOS. Transactions of the American Geophysical Union*, *84*, 38,377.

Zibordi, G., Holben, B., Slutsker, I., Giles, D., D'Alimonte, D., Melin, F., et al. (2009). AERONET-OC: A network for the validation of ocean color primary products. *Journal of Atmospheric and Oceanic Technology*, *26*, 1634–1650.

Zibordi, G., Melin, F., & Berthon, J. -F. (2006). Comparison of SeaWiFS, MODIS and MERIS radiometric products at a coastal site. *Geophysical Research Letters*, *33*. http://dx.doi.org/10.1029/2006GL025778.